Computer Science Department of The University of Auckland
CITR at Tamaki Campus (http://www.citr.auckland.ac.nz/)

CITR-TR-116 Sep 2002

Cylindrical Panoramic Cameras – From Basic Design to Applications

Fay Huang, Shou Kang Wei, Reinhard Klette, Georgy Gimelfarb [1]
Ralf Reulke, Martin Scheele, Karsten Scheibe [2]

Abstract

This paper reviews major steps in designing, producing and applying cylindrical panoramic cameras. Basically such a camera is characterized by rotating linear sensors capturing one image column at a time. Extremely high numbers of pixels per line allow capturing of super-high resolution panoramic images. These can be used for stereo visualisation and stereo reconstruction, as will be discussed in this paper.

1 Centre for Image Technology and Robotics, Tamaki Campus, Building 731, The University of Auckland, Morrin Road, Glen Innes, Auckland 1005, New Zealand.

2 German Aerospace Center DLR, Germany, Institute of Space Sensor Technology and Planetary Exploration, Rutherfordstrasse 2, D-12484 Berlin

Cylindrical Panoramic Cameras - From Basic Design to Applications

Fay Huang, Shou Kang Wei, Reinhard Klette, Georgy Gimelfarb
CITR, Computer Science Department
The University of Auckland
Tamaki Campus, Auckland, New Zealand

Ralf Reulke, Martin Scheele, Karsten Scheibe
German Aerospace Center DLR, Germany
Institute of Space Sensor Technology and Planetary Exploration,
Rutherfordstrasse 2, D-12484 Berlin

Abstract

This paper reviews major steps in designing, producing and applying cylindrical panoramic cameras. Basically such a camera is characterized by rotating linear sensors capturing one image column at a time. Extremely high numbers of pixels per line allow capturing of super-high resolution panoramic images. These can be used for stereo visualisation and stereo reconstruction, as will be discussed in this paper.

1 Introduction

In this section we briefly sketch basics of the architecture of panoramic cameras.

1.1 Model

A single-line line camera is geometrically characterized by a single optical (projection) center, denoted as **C**, and a 1D linear photon-sensing device (e.g. CCD). To acquire a cylindrical panoramic image, a slit camera rotates with respect to a fixed 3D axis (e.g. the rotation axis of a turntable) and captures slit images consecutively at equidistant angles. Each slit image contributes to a single column of the resulting panoramic image. The camera setup of the panorama acquisition is shown in Fig. 1. The off-axis distance R and principal angle ω remain constant during a panoramic image acquisition process.

1.2 Hardware

These type of camera models have been studied recently [4]. Fig. 1 (left) shows a single-line panorama camera (built at DLR) which may rotate part of, or full $360°$. This color camera produces images having 10,200 pixels, and a full $360°$ image has 55,000 columns for f = 60 mm which results in a single image of size 3.3 gigabytes. The radiometric dynamics is 14 bits and the signal to noise ratio is in the range of 8 bits. The acquisition time depends from the illumination conditions and is about 4 minutes. The whole equipment is portable and is working with a typical car battery.

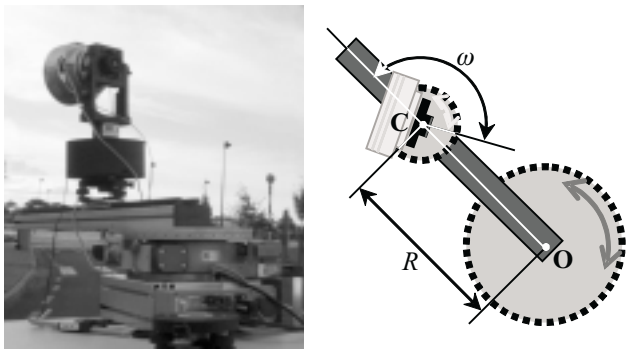

Figure 1. Camera setup for panoramic image acquisition.

2 Calibration

Panoramic cameras are of increasing importance for various applications in computer vision, computer graphics or robotics. Previously developed camera calibration methods (for 'standard' camera architectures following the pinhole camera model) are not applicable due to the non-linearity of the panoramic camera, defined by the existence of multiple (nonlinear) optical centers and a cylindrical image manifold.

First, camera calibration method using production-site facilities is discussed. Since it is not available for the end users and the values of R and ω are dynamically specified according to different scene range of interest, an on-site camera calibration method utilizing geometric properties available in real scenes is discussed next.

2.1 Production Site

The CCD-line cameras requires an extensive geometric and radiometric calibration procedure and concerns only the camera-head. The main result of the geometric calibration procedure are the accurate pixel coordinates in the focal plane in relation to the optical axis (interior orientation). Additional results is the spatial dependent point-spread function (PSF), which is related to image resolution and image quality. Ideal parameters (e.g. the focal length f) for characterization of the systems can be derive from this measurements. Radiometric calibration is related to the signal-to-noise-ratio (SNR), signal dynamics and linearity as well as true-color retrieval. Additional measurements concerns the homogeneous of the signal, e.g. photo-response non-uniformity (PRNU) and dark-signal non-uniformity (DSNU). All measurements will be done in a special calibration facility.

2.2 On-site

In this subsection, we focus on the calibration of the two dominant parameters that characterize the camera model, R and ω. The main intention is to find a single linear equation that links 3D geometric scene features to the camera model such that by providing sufficient scene measurements or knowledge (such as distances or lengths) we are able to calibrate accurately the values of R and ω.

We assume there are at least three straight line segments in the captured real scene (e.g. a special object with straight edges), which are all parallel to the rotation axis. The length of these line segments and the distances[1] between any two parallel lines are measurable.

[1] The distance between two parallel lines is the length of a line segment that connects both lines and which is perpendicular to these lines.

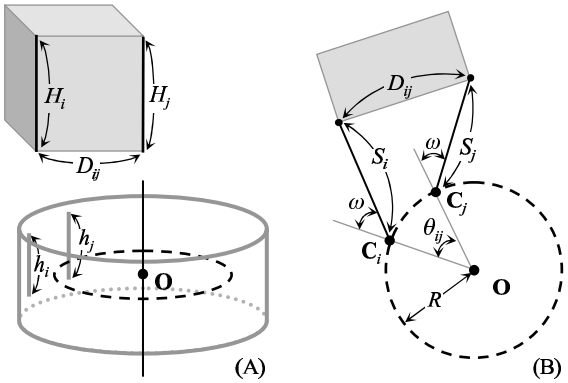

Figure 2. Camera calibration utilizing the parallel line segments in the 3D scene.

Consider a pair of parallel line segments of lengths H_i and H_j in 3D space as shown in Fig. 2(A). The length of a projection of the line segments on image columns can be determined from the input image, denoted as h_i and h_j in pixels respectively. The distance between these two parallel lines is denoted as D_{ij}.

Figure 2(B) shows the top view of the geometry. The camera optical centers that see these two parallel lines are denoted as $\mathbf{C}_i$ and $\mathbf{C}_j$ respectively. The distances S_i and S_j are defined to be the shortest distances between the associated camera optical centers and the parallel lines respectively, and can be calculated by the following relations

$$S_i = \frac{fH_i}{h_i} \text{ and } S_j = \frac{fH_j}{h_j},$$

where f is the pre-calibrated effective focal length of the (line-)camera. The angular distance θ_{ij} ($\angle\, \mathbf{C}_i\mathbf{O}\mathbf{C}_j$) can be calculated as follows:

$$\theta_{ij} = \frac{2\pi d_{ij}}{W},$$

where d_{ij} is the distance between two projections of the parallel lines on image, measured in pixel, and W is the width of a panorama in pixels.

We obtain a linear equation as follows:

$$\begin{aligned} 0 &= (1-\cos\theta_{ij})R^2 \\ &+ (S_i+S_j)(1-\cos\theta_{ij})R\cos\omega \\ &- (S_i-S_j)\sin\theta_{ij}R\sin\omega \\ &+ \frac{S_i^2+S_j^2-D_{ij}^2}{2} - S_iS_j\cos\theta_{ij}. \end{aligned} \quad (1)$$

Since the values of S_i, S_j, D_{ij}, and θ_{ij} are known, the equation can be arranged into the following form,

$$K_1X_1 + K_2X_2 + K_3X_3 + K_4 = 0,$$

where $K_i, i = 1, 2, 3, 4$, are coefficients. The three linearly independent variables are

$$\begin{aligned} X_1 &= R^2 \\ X_2 &= R\cos\omega \quad \text{and} \\ X_3 &= R\sin\omega. \end{aligned}$$

Because of the dependency among the variables X_1, X_2, and X_3, there are multiple solutions of R and ω, if we solve it by linear least-square technique. To tackle this multiple-solutions problem, we may constrain the parameter estimation further by the inter-relation among X_1, X_2, and X_3, which is

$$X_1^2 = X_2^2 + X_3^2$$

because of

$$R^2 = (R\cos\omega)^2 + (R\sin\omega)^2.$$

Assume that n equations are given. We want to minimize the following:

$$min \sum_{i=1}^{n} \left(K_{1n}X_1 + K_{2n}X_2 + K_{3n}X_3 + K_{4n}\right)^2, \qquad (2)$$

subject to the equality constraint $X_1 = X_2^2 + X_3^2$, where the values of $K_{in}, i = 1, 2, 3, 4$, are calculated based on the measurements from real scenes and the image, and $X_1 = R^2$, $X_2 = R\cos\omega$, and $X_3 = R\sin\omega$. Now, the values of R and ω can be found uniquely by

$$R = \sqrt{X_1}$$

and

$$\omega = \arccos\left(\frac{X_2}{\sqrt{X_1}}\right).$$

Note that even though the additional constraint forces that a non-linear optimization method to be used, the expected linear parameter estimation quality remains.

3 Stereo Visualization

We discuss two possible applications of symmetric panoramic images captured with angles ω and $-\omega$ during one rotation of the panoramic camera. We start with stereo visualization in this section.

3.1 Spatial Sampling

Spatial sampling describes how a 3D space is sampled without considering underlining structures or the complexity of 3D scenes. Studies of spatial sampling for image acquisition are of great importance for vision applications.

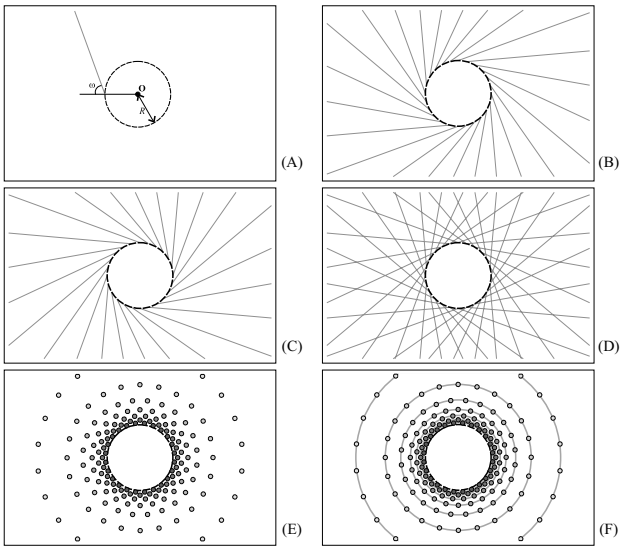

Figure 3. Sampling structure in the outward case.

A spatial sample is defined by intersections of projection rays. Figure 3 illustrates top views of spatial sample formations of a stereo panoramic pair. The camera model is depicted in Fig. 3(A). Projection rays emitting panoramically from projection centers on the base circles, are shown in Fig. 3 (B) and (C) for the right and left stereo panoramas, respectively. Superimposing Fig. 3 (B) and (C), we have Fig. 3 (D) which reveals the basic structure of stereo samples, that is, the concentric circles formed by the intersections of the projection rays.

Figure 3 (E) removes the projection rays in Fig. 3 (D), and replaces the intersections by small colored circles (the darker the closer to **O**). In Fig. 3 (F), the sampling structure are augmented with supporting concentric circles in gray. Note that the innermost dashed black circle is the base circle; one should not confuse it with the supporting concentric circles. Radiuses of the concentric circles increase non-linearly. The 'concentric circles' are indeed concentric cylinders in 3D. Motivated by the fact that samples are layered in depth (the distance from **O**), we refer to these concentric circles (cylinders in 3D) as *depth layers*.

The 3D visualization of a sampling structure corresponding to Fig. 3 (F) is depicted in Fig. 4. The samples are drawn at different sizes (i.e. larger as they are further away from **O**) and at different colors for different depth layers. Only samples of $240°$ views are shown for clearness. The structure of depth layers can be described by a set of equal-height concentric cylinders whose tops and bottoms are cut-off by a pair of co-axis hyperboloid symmetric to the base plane. The observation can also be confirmed by the fact that the

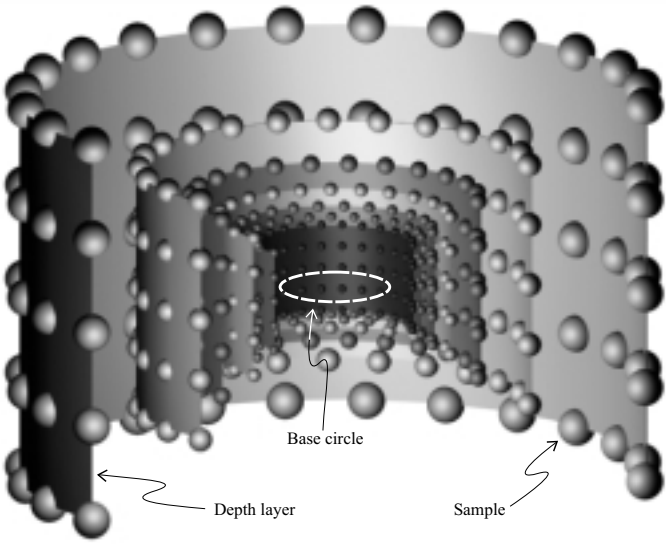

Figure 4. A 3D view of sampling structure in outward case.

epipolar surface for stereo panoramas is a half-hyperboloid [8]. This observation helps in further modeling for studying geometric relations of scenes, application constraints and acquisition systems.

Since the diversity of sample densities and density distributions is influenced by the range of ω and possible R values, it is not difficult to infer the advantageous flexibility of the acquisition model permitting an advanced control of spatial sampling over a dynamic range of scenes. This consequence motivates us further to study these two camera parameters, especially for image quality control and the camera analysis and design problems, which will be discussed in the later subsection.

Sampling resolution is defined as the total number of samples in 3D space. It gives a measure of sampling density and characterizes spatial sampling in a general sense. We have the following theorem.

Theorem 3.1 *Given a pair of stereo panoramas of image resolution $W \times H$, and the value of the associated principal angle of both images is ω, where $\omega \in (0°, 180°)$. The total number of spatial samples, namely spatial sampling resolution of the stereo panoramas, is equal to*

$$W \times H \times \left\lfloor \frac{\omega W}{180°} \right\rfloor . \tag{3}$$

Consider a pair of stereo panoramas, when the value of the associated principal angle ω equals to $0°$ or $180°$, there is no sample. The value of the off-axis distance R of a stereo panorama pair has no impact onto the spatial sampling resolution. The spatial sampling resolution of a stereo panoramic pair increases as the value of the associated ω increases in the range $(0°, 180°)$. In the outward case, i.e. $0° < \omega \leq 90°$, the spatial sampling resolution of a stereo panoramic pair reaches to the maximum when the associated principal angle $\omega = 90°$, that consists with the results in [9].

3.2 Quality Control

We denote by *image quality control* a method which ensures proper configurations of camera settings such that image quality meets the requirements or criteria defined by an application under the assumption that a capable and accurate camera system is used. The development of such an image quality control method requires a basic understanding of geometric and/or photometric relations among the camera system, 3D scene complexities, and application requirements.

In this paper, two main quality control problems of stereo panorama imaging are discussed. They are *scene composition* and *stereo acuity*. The scene composition problem is concerned about how the camera's parameter values should be set such that the intended scenes or subjects are composed desirably in resultant images, without involving any subjective issues of scene composition. Without a proper control of scene composition, the resultant images may miss important features, might be inexpressive for the subjects, or may possibly cause ambiguities or incoherence.

The stereo acuity control is to analyze how the camera parameters can be set such that the resultant number of depth layers meet the stereo acuity requirement in an application, for a specified family of scenes of interest. Insufficient stereo acuity over the relevant interval of distance values for a given 3D scene of interest produces a *cardboard effect* [13], i.e. the 3D scene is perceived as a set of 'parallel cardboards', sorted in depth, one sitting in front of the next one. On the other hand, stereo acuity greater than the upper disparity limit of human vision causes double images, called *dipopia*, which results in uncomfortable stereoscopic viewing as well as eyestrain [12, 10, 3, 5].

Four parameters are introduced. The first two parameters describe the range of scenes of interest by D_1 and D_2 as nearest and furthest distances from **O** where the quality control is applied to. And the third parameter H_1 is defined by the distance between an optical center **C** and a point on the base plane in distance D_1 from **O**; we call it *distance to target range*. The last parameter θ_w is the width of the angular disparity interval for the nearest and furthest 3D points in the range of scenes of interest with respect to **O**.

Now we assume that values of these four parameters D_1, D_2, H_1, and θ_w are specified with respect to the intended scenes and the application particulars. What values of camera parameters, i.e. off-axis distance R and principal angle

ω, should be chosen such that the demanded quality of scene composition and the stereo acuity can be realized? We answer this question in the following theorem.

Theorem 3.2 *While the parameters D_1, D_2, H_1, and θ_w are bounded, there exists a unique solution for both off-axis distance R and principal ω satisfying the geometric constraints of scene composition and stereo acuity for a stereoscopic panoramic camera:*

$$R=\sqrt{D_1^2+H_1^2+2D_1H_1\frac{D_1-D_2\cos\left(\frac{\theta_w}{2}\right)}{\sqrt{D_1^2+D_2^2-2D_1D_2\cos\left(\frac{\theta_w}{2}\right)}}}$$

and

$$\omega=\arccos\left(\frac{D_1D_2\cos\left(\frac{\theta_w}{2}\right)-D_1^2-H_1\sqrt{A}}{\sqrt{A(D_1^2+H_1^2)+2D_1H_1(D_1-D_2\cos\left(\frac{\theta_w}{2}\right))\sqrt{A}}}\right),$$

where $A=(D_1^2+D_2^2-2D_1D_2\cos\left(\frac{\theta_w}{2}\right))$.

Since the solution for the camera parameters is unique, neither the camera parameter R nor ω can satisfy the stereoscopic panorama quality requirement adequately alone. Using the computed control values, the image quality of stereoscopic panoramas with respect to scene composition and stereo acuity criteria can be ensured at acquisition time. As only three on-site measures are required (i.e. D_1, D_2, H_1) the overheads in addition to the original imaging process are acceptable.

4 Stereo Image Analysis

The second application of symmetric panoramic images is depth or shape recovery.

4.1 Epipolar Geometry

The study of epipolar geometry is essential for the applications such as 3D reconstruction from panoramic images, visualization or simulation of walk-through, i.e. the virtual paths created between multiple panoramas. The epipolar curve equation serves as a fundamental tool for many important computer vision tasks, such as pose estimation and stereo analysis.

The general epipolar curve equation for a pair of arbitrary polycentric panoramas is presented by the following theorem.

Theorem 4.1 *Let (x_1, y_1) and (x_2, y_2) denote the image coordinates of the projection of a 3D point in the source image $E_{\mathcal{P}_1}$ and the destination image $E_{\mathcal{P}_2}$, respectively. Consider x_1 and y_1 as being given. Let $\alpha_1=\frac{2\pi x_1}{\mu W_1}$, $\alpha_2=\frac{2\pi x_2}{\mu W_2}$, $\delta_1=(\alpha_1+\omega_1)$, $\delta_2=(\alpha_2+\omega_2)$, and $\beta_1=\arctan(\frac{y_1}{f_1})$. The corresponding epipolar curve on the destination image $E_{\mathcal{P}_2}$ cab be represented by the equation*

$$y_2=\frac{f_2\boldsymbol{r}_2^T\cdot\boldsymbol{V}}{\sin\delta_2\boldsymbol{r}_1^T\cdot\boldsymbol{V}+cos\delta_2\boldsymbol{r}_3^T\cdot\boldsymbol{V}-R_2\cos\omega_2},$$

which is only valid if the value of the denominator is greater than zero. The vector $\boldsymbol{V}$ is defined as follows:

$$\boldsymbol{V}=\boldsymbol{A}+\frac{R_2\sin\omega_2+\cos\delta_2\boldsymbol{r}_1^T\cdot\boldsymbol{A}-\sin\delta_2\boldsymbol{r}_3^T\cdot\boldsymbol{A}}{\sin\delta_2\boldsymbol{r}_3^T\cdot\boldsymbol{B}-\cos\delta_2\boldsymbol{r}_1^T\cdot\boldsymbol{B}}\boldsymbol{B},$$

where

$$\boldsymbol{A}=\begin{pmatrix}R_1\sin\alpha_1-t_x\\-t_y\\R_1\cos\alpha_1-t_z\end{pmatrix}\ \textit{and}\ \boldsymbol{B}=\begin{pmatrix}\sin\delta_1\cos\beta_1\\\sin\beta_1\\\cos\delta_1\cos\beta_1\end{pmatrix}.$$

Furthermore, the matrix $[\boldsymbol{r}_1^T\boldsymbol{r}_2^T\boldsymbol{r}_3^T]^T$ and the vector $(t_x,t_y,t_z)^T$ specify the orientation and the position of the panoramic camera of $E_{\mathcal{P}_2}$ with respect to the camera coordinate system of the panoramic camera of $E_{\mathcal{P}_1}$.

An intuitive and practical way to reduce the dimensionality of the general epipolar curve equation is to make all the associated axes of the panoramas leveled to the sea level. It can be achieved by mounting the camera on a leveled tripod. A polycentric panoramic pair whose associated axes are orthogonal to the sea level is called *leveled panoramic pair*.

Note that the heights of images in a leveled panoramic pair can be different. Under the assumption that a panoramic pair is perfectly leveled, the general epipolar curve equation in Theorem 4.1 can be simplified. We have the following corollary.

Corollary 4.2 *Let (x_1, y_1) and (x_2, y_2) be a pair of corresponding image points in a pair of leveled polycentric panoramas $E_{\mathcal{P}_1}(R_1, f_1, \omega_1, \gamma)$ and $E_{\mathcal{P}_2}(R_2, f_2, \omega_2, \gamma)$, respectively. Given x_1 and y_1, the epipolar curve equation in this case can be simplified as follows:*

$$y_2=\frac{y_1\left(\frac{f_2}{f_1}\right)\boldsymbol{K}-t_yf_2\sin(\sigma_2-\sigma_1)}{R_2\sin(\sigma_1-\alpha_2-\phi)-R_1\sin\omega_1-t_x\cos\sigma_1+t_z\sin\sigma_1},$$

where $\alpha_1=\frac{2\pi x_1}{\mu W_1}$, $\alpha_2=\frac{2\pi x_2}{\mu W_2}$, $\sigma_1=(\alpha_1+\omega_1)$, $\sigma_2=(\alpha_2+\omega_2+\phi)$, the angle ϕ determines the rotation with respect to the y-axis, and $\boldsymbol{K}=R_2\sin\omega_2-R_1\sin(\sigma_2-\alpha_1)-t_x\cos\sigma_2+t_z\sin\sigma_2$.

Two panoramas whose axes coincide are called a *co-axis panoramic pair*. This constraint reduces two rotational and two translational parameters, and yet has its practical merit. The epipolar curves of a co-axis pair coincide with image columns under some camera setting assumptions. Also note

that the implementation of such a configuration is reasonably straightforward. A normal tripod allows such a setting. Therefore, this geometrical constraint has been commonly applied in some panoramic camera architectures such as the catadioptric approach [11, 2, 6, 7].

The epipolar geometry of a co-axis panoramic pair is characterized in the following corollary.

Corollary 4.3 *Let* (x_1, y_1) *and* (x_2, y_2) *be a pair of corresponding image points in a co-axis pair of panoramas. Given* x_1 *and* y_1*, we have*

$$y_2 = \frac{y_1 \left(\frac{f_2}{f_1}\right)(R_2 \sin\omega_2 - R_1 \sin(\sigma_2 - \alpha_1)) - t_y f_2 \sin(\sigma_2 - \sigma_1)}{R_2 \sin(\sigma_1 - \alpha_2 - \phi) - R_1 \sin\omega_1},$$

where $\alpha_1 = \frac{2\pi x_1}{\mu W_1}$, $\alpha_2 = \frac{2\pi x_2}{\mu W_2}$, $\sigma_1 = (\alpha_1 + \omega_1)$ *and* $\sigma_2 = (\alpha_2 + \omega_2 + \phi)$*, and the angle* ϕ *determines the rotation with respect to the y-axis.*

Figure 5 illustrates the distinctiveness of epipolar curve patterns in four different geometric configurations: leveled; concentric; symmetric; and single-center panoramas.

4.2 Stereo Matching

Due to the known epipolar curves, the panoramic pair can be easily brought to the standard horizontal epipolar stereo pair having one-to-one correspondence between the pixel rows in the both images. Assuming a continuous visible surface, binocular stereo reconstruction of the panoramic scene can be obtained by one or another conventional stereo technique, e.g., by symmetric dynamic programming stereo (SDPS) [1].

Figures 6 and 7 show the left and right stereo images of a close-range urban 3D scene and results of 3D stereo reconstruction with the SDPS (namely, the range image grey-coding the depths and the ortho image fusing the stereo images in accord with visibility of the reconstructed 3D points).

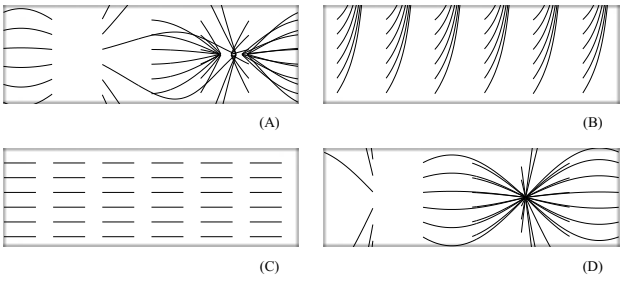

Figure 5. Epipolar curves of four special cases: (A) leveled; (B) concentric; (C) symmetric; and (D) single-center panoramas.

Figure 6. Stereo pair of panoramic images brought to the standard epipolar geometry by rectifying the epipolar curves.

Figure 7. Range and ortho images of the reconstructed 3D scene.

Some reconstruction errors, e.g. on the sky or near the rightmost columns of the building are typical for these panoramic line cameras. Because of relatively long time for capturing a single image, the left and right images of the stereo pair differ considerably in all the "dynamically changing" areas such as cloud patterns or positions of moving people.

5 Conclusion

We reviewed recent developments in fundamentals and production of cylindrical panoramic cameras. Major 'milestones' have been set, but future research and design has to address more specific questions. For example, the impact of inaccurate rotations on epipolar geometry is one of these subjects, and the unification of several 3D distance maps produced by several stereo pairs of symmetric panoramic images is another (difficult) subject.

References

[1] G. Gimel'farb. Probabilistic regularisation and symmetry in binocular dynamic programming stereo. *PRL*, 23(4):431–442, February 2002.

[2] J. Gluckman, S. Nayar, and K. Thorek. Real-time panoramic stereo. In *Proc. DARPA'98*, pages 299–303, Monterey, California, USA, Novemeber 1998.

[3] W. A. Ijsselsteijn, H. de Ridder, and J. Vliegen. Effects of stereoscopic filming parameters and display duration on the subjective assessment of eye strai. In *Proc. SDVRS VII*, pages 12–22, San Jose, California, USA, January 2000.

[4] R. Klette, G. Gimel'farb, and R. Reulke. Wide-angle image acquisition, analysis and visualization. In *Proc. 14th Internat. Conf. "Vision Interface" (VI'2001)*, pages 114–125, Ottawa, Canada, June 2001.

[5] U. Mayer, M. Neumann, W. Kubbat, and K. Landau. Is eye damage caused by stereoscopic displays? In *Proc. SDVRS VII*, pages 4–11, San Jose, California, USA, January 2000.

[6] S. Nene and S. Nayar. Stereo with mirrors. In *ICCV98*, pages 1087–1094, January 1998.

[7] R. Petty, M. Robinson, and J. Evans. 3d measurement using rotating line-scan sensors. *Measurement Science and Technology*, 9(3):339–346, 1998.

[8] S. Seitz. The space of all stereo images. In *Proc. ICCV'01*, pages 26–33, Vancouver, Canada, July 2001.

[9] H. Shum, A. Kalai, and S. Seitz. Omnivergent stereo. In *Proc. ICCV'99*, pages 22–29, Korfu, Greece, September 1999.

[10] M. Siegel, Y. Tobinaga, and T. Akiya. Kinder gentler stereo. In *SPIE Proc. Stereoscopic Displays and Applications X*, pages 18–27, San Jose, California, USA, January 1999.

[11] D. Southwell, J. Reyda, M. Fiala, and A. Basu. Panoramic stereo. In *ICPR'96*, pages A:378–382, August 1996.

[12] E. Viire. Health and safety issues for vr. *Communications of the ACM*, 40(8):40–41, 1997.

[13] H. Yamanoue, M. Okui, and I. Yuyama. A study on the relationship between shooting conditions and cardboard effect of stereoscopic images. *IEEE Tran. on Circuits and Systems for Video Technology*, 10(3):411–416, 2000.